Cite as: V. H. Cornejo *et al.*, *Science* 10.1126/science.abg0501 (2021).

Voltage compartmentalization in dendritic spines in vivo

Victor Hugo Cornejo, Netanel Ofer, Rafael Yuste*

Neurotechnology Center, Department of Biological Sciences, Columbia University, New York, NY 10027, USA.

***Corresponding author. Email: rmy5@columbia.edu**

Dendritic spines mediate most excitatory neurotransmission in the nervous system, so their function must be critical for the brain. Spines are biochemical compartments, but could also electrically modify synaptic potentials. Using two-photon microscopy and a genetically-encoded voltage indicator, we measured membrane potentials in spines and dendrites from pyramidal neurons in somatosensory cortex of mice during spontaneous activity and sensory stimulation. Spines and dendrites were depolarized together during action potentials, but, during subthreshold and resting potentials, spines often experienced different voltages than parent dendrites, even activating independently. Spine voltages remained compartmentalized after two-photon optogenetic activation of individual spine heads. We conclude that spines are elementary voltage compartments. The regulation of voltage compartmentalization could be important for synaptic function and plasticity, dendritic integration, and disease states.

Dendritic spines are small protrusions that cover dendrites of neurons (*1*) and mediate most excitatory connections in the brain (*2–4*). Aside from connecting neurons, they must play an additional role, since excitatory axons specifically target spines, avoiding dendritic shafts (*5*). Spine morphologies, with a small (~1 μm in diameter) head connected to the dendrite by a thin (~140 nm in diameter) neck, suggest that they isolate synapses from the dendrite. Indeed, spines are calcium compartments (*6*, *7*) that biochemically isolate synaptic inputs, enabling input-specific plasticity (*8*, *9*). However, calcium compartmentalization also occurs in aspiny dendrites (*10*, *11*), so spines may implement additional functions. One possibility is that spines are also electrical compartments (*12–15*). While dendritic voltages should fully invade the spine, synaptic potentials could attenuate as they propagate from the spine toward the parent dendrite (*13*, *16*, *17*). If spines were electrical compartments, the local depolarization at the spine caused by synaptic potentials could be significantly higher than what is measured at the dendrite or soma (*18*).

The introduction of optical methods has enabled measurements of membrane potential of spines in vitro using organic dyes or genetically-encoded voltage indicators (GEVIs) (*19*). Although the invasion of action potentials (APs) into spines has been demonstrated (*20–23*), optical measurements of the electrical responses of spines to synaptic inputs have been inconsistent, with some studies finding similar potentials in spines and dendrites (*21*) while others find larger depolarizations in spines (*22*, *23*). Experiments with two-photon photobleaching or glutamate uncaging have been used to estimate the degree of electrical compartmentalization of spines, with a variety of results (*24–31*). Consistent with voltage compartmentalization, nanopipettes recordings from spines in brain slices reveal large amplitude synaptic potentials (*32*). However, these experiments examined spines in vitro, so the electrical behavior of spines during physiological states remains unexplored.

To investigate the electrical function of spines in vivo, we developed a GEVI that could be efficiently excited with two-photon illumination, and expressed it in pyramidal neurons from layer 2/3 mouse somatosensory cortex. This sensor, postASAP (short for 'post-synaptic ASAP'), used an ASAP (Accelerated Sensor of APs) GEVI backbone (*33*), modified with mutations for enhanced sensitivity and a PSD95.FingR nanobody domain to enrich its expression in spines (*34*, *35*) (Fig. 1A; see supplementary text). To express postASAP in vivo, we used *in utero* electroporation to achieve sparse yet robust expression, and measured the co-expression of postASAP and red fluorescent protein (RFP) (Fig. 1B and fig. S2A). The soluble RFP showed higher fluorescence in larger volume compartments (fluorescence ratio soma/spine=3.02 ± 1.89, soma/dendrite=2.09 ± 1.84, dendrite/spine=1.45 ± 1.21, mean±std; $p<0.0001$, Kruskal-Wallis; fig. S2B). Meanwhile, postASAP fluorescence levels were evenly distributed among neuronal compartments (ratio soma/spine=0.98 ± 0.59, soma/dendrite=1.04 ± 0.58, dendrite/spine=0.95 ± 0.62, mean±std; $p=0.40$, Kruskal-Wallis), indicating membrane targeting, with robust labeling of dendrites and spines. To investigate the biophysical properties of postASAP, we first analyzed the fluorescence-voltage (F-V) relation with two-photon excitation in cultured ND7/23 cells (Fig. 1C). F-V curves were fitted with a Boltzmann function and displayed linearity in the range of -100 and -40 mV. To calibrate postASAP signals in vivo, we used whole-cell patch clamp recordings and, simultaneously, two-photon imaging of postASAP in neuronal somata (Fig. 1D), finding a clear correspondence between electrical activity and fluorescence (Fig. 1E).

Changes in fluorescence correlated with subthreshold depolarizations, rather than with APs (Fig. 1, E and F; see supplementary text), as expected from the low-pass behavior of the voltage sensor and imaging rate (~16 ms/frame). Within subthreshold depolarizations, the relation between voltage and changes in fluorescence was fitted by a linear function with a slope of 1.71 ± 0.02 mV/-ΔF/F % (slope±sem, p<0.0001) (Fig. 1G), similar to the linear range of the in vitro F-V curve (1.67 mV/-ΔF/F %).

We then used two-photon imaging in vivo to measure the voltage dynamics experienced by basal dendrites and their spines from neurons expressing postASAP, while performing simultaneous somatic whole-cell recordings (Fig. 2A; see supplementary text). During spontaneous activity, we found three spatiotemporal patterns of depolarizations in dendritic trees (Fig. 2B and movie S1). In the first spatial pattern ('AP'), occurring during trains of APs, dendrites and spines were synchronously depolarized (Fig. 2, B and C). Peak depolarizations during APs were similar in spines and adjacent dendrites, confirming the functional expression of postASAP in spines and reports of AP invasion into spines without failures or decrement (*6*, *7*, *20*, *36*, *37*) (Fig. 2, D and E; spine=20.0 ± 9.5 mV, dendrite=21.3 ± 9.9 mV, mean±std; p=0.24, Mann-Whitney). Interestingly, in the absence of APs, during subthreshold potentials or even in the absence of significant somatic depolarization in the whole-cell recordings, two other spatial types of depolarization were observed (Fig. 2, B and C). In a second spatial pattern ('Dendrite+Spines'), localized segments of dendrites with associated spines were depolarized together (Fig. 2F; spine=15.9 ± 5.8 mV, dendrite=15.3 ± 5.6 mV, mean±std; p=0.3767, Mann-Whitney). We also observed a third pattern ('Spine-only'), where individual spines became depolarized independently, or with a reduced depolarization of the parent dendrite, presumably reflecting isolated synaptic events (Fig. 2G; spine=15.0 ± 7.2 mV, dendrite=6.97 ± 4.2 mV, mean±std; p<0.0001, Mann-Whitney). The two last patterns were found more frequently during somatic subthreshold events (fig. S8 and supplementary text). Spine voltage peaks reached by Spine-only events ranged from 5.0 to 39.8 millivolts, although this might represent an overestimate, due to the difficulty of measuring smaller depolarizations with sufficient SNR (fig. S4A and supplementary text).

Next, we wondered what spatial patterns of depolarizations were found after sensory stimulation. We used air puffs to activate the whiskers, while simultaneously imaging postASAP in dendrites and spines (Fig. 3A; see supplementary text), and also found APs (fig. S7, C and D, and movie S2), Dendrite+Spines, and Spine-only patterns (Fig. 3, B and C). After sensory stimulation, Dendrite+Spines events (Fig. 3D; spine=13.7 ± 5.5 mV, dendrite=13.0 ± 5.4 mV, mean±std; p=0.1299, Mann-Whitney) were detected more frequently, whereas Spine-only events did not change significantly (fig. S8 and supplementary text). Spine-only patterns (Fig. 3E; spine=12.8 ± 5.4 mV, dendrite=7.5 ± 4.5 mV, mean±std; p<0.0001, Mann-Whitney) had similar peak amplitudes to those during spontaneous activity. All dendritic and spine depolarizations were reversibly blocked by synaptic antagonists (fig. S9 and supplementary text), confirming their physiological nature.

We then turned our attention to the Spine-only patterns, where spines activated independently. To explore this, we activated spine heads or dendritic segments using two-photon optogenetics (*38*) with ChrimsonR (*39*) (Fig. 4A; see supplementary text), while simultaneously measuring their voltages with postASAP (Fig. 4B). For calibration, we imaged postASAP in the soma during two-photon optogenetic activation (Fig. 4C), finding a gradual fluorescence response, proportional to laser power (fig. S12A). In vivo patch-clamp indicated reliable optogenetic responses and allowed us to measure the peak currents generated by the photostimulation (Fig. 4D). We then photostimulated small segments of dendrites while measuring postASAP fluorescence in dendrites and spines, finding similar depolarizations in dendrites and adjacent spines (Fig. 4E; spine=8.1 ± 4.2 mV, dendrite=7.6 ± 4.0 mV, mean±std; p=0.55, Mann-Whitney). Finally, we photostimulated spine heads, to mimic synaptic potentials, finding depolarizations that decreased as they spread into the parent dendrites (Fig. 4F; spine=11.2 ± 3.6 mV, dendrite=6.0 ± 2.2 mV, mean±std; p<0.0001, Mann-Whitney). These optogenetic results were in agreement with our measurements during spontaneous or sensory-evoked activity (Figs. 2 and 3), confirming voltage attenuation from spine-to-dendrite, but no attenuation from dendrite-to-spine. This asymmetric, diode-like, electrical behavior is expected from cable properties (*13*, *16*).

To estimate the electrical properties of the spines, we used a simplified steady-state electrical equivalent circuit (*30*, *40*) (Fig. 4G), with a very small (<0.01 pF) spine capacitance, so synaptic currents flow through the spine neck resistance (R_n). Defining the spine input resistance (R_{sp}) as the sum of R_n and the dendritic input resistance (R_{den}):

$$R_{sp} = R_n + R_{den} \quad (1)$$

According to Ohm's law, R_{sp} depends on the current flowing across the synapse (I_{syn}) and the voltage in the spine (V_{sp}):

$$R_{sp} = \frac{V_{sp}}{I_{syn}} \quad (2)$$

Applying the voltage divider equation, one finds:

$$\frac{R_n}{R_{den}} = \frac{V_{sp}}{V_{den}} - 1 \quad (3)$$

As we obtained a similar average resistance ratio (R_n/R_{den}) for Spine-only events during spontaneous activity and

sensory stimuli, and also for optogenetically stimulated spines (Fig. 4H; 1.7 ± 2.8; 2.1 ± 5.9; 1.1 ± 0.8, respectively, mean±std; p=0.34, Kruskal-Wallis), R_n would be equivalent to R_{den} for most spines (*29*). To estimate R_n, we solved Eq. 1, 2, and 3, obtaining:

$$R_n = \frac{V_{sp} - V_{den}}{I_{syn}} \quad (4)$$

and assuming an I_{syn}=22.7 pA for photostimulated spines (Fig. 4D), we obtained an average R_n of 226.6 ± 128.8 MΩ (mean±std), ranging from ~0 to 530.8 MΩ (Fig. 4I; see supplementary text), in line with previous estimates with different methods (*29*, *30*, *32*).

Our results demonstrate that measurements of spine depolarization in vivo are feasible with two-photon GEVI imaging, providing an initial glimpse into the complex spatiotemporal patterns of depolarizations of dendrites and spines during spontaneous activity or sensory stimulation. Consistent with previous reports (*6*, *7*, *20–22*), we found synchronous depolarization of dendrites and spines during backpropagation of axonal APs into dendrites and spines (AP pattern). In addition, we detected local and transient depolarizations of dendritic segments and their spines (Dendrite+Spines pattern), likely corresponding to a combinatory of synaptic potentials and dendritic spikes (*41–44*). Importantly, we also found individual spines activating independently (Spine-only pattern), even in the absence of significant dendritic or somatic activity. These spine-independent depolarizations likely represent individual synaptic potentials, due to their occurrence during subthreshold synaptic inputs, their spatial restriction and their sensitivity to synaptic blockers (*6*, *7*, *45*, *46*). These synaptic depolarizations of spines can be large in amplitude, at least of tens of millivolts (*16*, *32*, *47–49*). The presence of spine-independent depolarization during spontaneous and sensory evoked activity implies that spines can compartmentalize voltage in physiological states in vivo. Indeed, using two-photon optogenetic activation of individual spines, we demonstrated this directly, while also revealing that dendritic potentials propagated into spines faithfully. Thus, our data indicate that the spines act as diodes, with no attenuation of dendritic potentials or AP, but significant attenuation of synaptic potentials (*13*, *16*), maintaining a voltage gradient with the dendrite (*50*, *51*). The mechanisms underlying spine voltage compartmentalization could involve geometrical and ultrastructural factors, passive cable properties, voltage-sensitive ion channels and synaptic receptors (*18*). Regardless of the mechanism, our results show that dendritic spines, in addition to serving as biochemical compartments, are also elementary electrical compartments for synapses. The regulation of the voltage compartmentalization of synaptic inputs by spines could be important for synaptic function (*52*) and plasticity (*8*, *53*), dendritic integration (*54*), and be affected in mental and neurological diseases (*55*).

REFERENCES AND NOTES

1. S. Ramon y Cajal, Estructura de los centros nerviosos de las aves. *Rev. Trim. Histol. Norm. Patol.* **1**, 1–10 (1888).
2. E. G. Gray, Electron microscopy of synaptic contacts on dendrite spines of the cerebral cortex. *Nature* **183**, 1592–1593 (1959). doi:10.1038/1831592a0 Medline
3. K. M. Harris, S. B. Kater, Dendritic spines: Cellular specializations imparting both stability and flexibility to synaptic function. *Annu. Rev. Neurosci.* **17**, 341–371 (1994). doi:10.1146/annurev.ne.17.030194.002013 Medline
4. R. Yuste, *Dendritic Spines* (MIT Press, 2010).
5. A. Peters, I. R. Kaiserman-Abramof, The small pyramidal neuron of the rat cerebral cortex. The perikaryon, dendrites and spines. *Am. J. Anat.* **127**, 321–355 (1970). doi:10.1002/aja.1001270402 Medline
6. R. Yuste, W. Denk, Dendritic spines as basic functional units of neuronal integration. *Nature* **375**, 682–684 (1995). doi:10.1038/375682a0 Medline
7. X. Chen, U. Leischner, N. L. Rochefort, I. Nelken, A. Konnerth, Functional mapping of single spines in cortical neurons in vivo. *Nature* **475**, 501–505 (2011). doi:10.1038/nature10193 Medline
8. J. C. Magee, D. Johnston, A synaptically controlled, associative signal for Hebbian plasticity in hippocampal neurons. *Science* **275**, 209–213 (1997). doi:10.1126/science.275.5297.209 Medline
9. S. J. Lee, Y. Escobedo-Lozoya, E. M. Szatmari, R. Yasuda, Activation of CaMKII in single dendritic spines during long-term potentiation. *Nature* **458**, 299–304 (2009). doi:10.1038/nature07842 Medline
10. J. H. Goldberg, G. Tamas, D. Aronov, R. Yuste, Calcium microdomains in aspiny dendrites. *Neuron* **40**, 807–821 (2003). doi:10.1016/S0896-6273(03)00714-1 Medline
11. G. J. Soler-Llavina, B. L. Sabatini, Synapse-specific plasticity and compartmentalized signaling in cerebellar stellate cells. *Nat. Neurosci.* **9**, 798–806 (2006). doi:10.1038/nn1698 Medline
12. W. Rall, in *Excitatory Synaptic Mechanisms, Proceedings of the Fifth International Meeting of Neurobiologists*, P. Andersen, J. Jansen, Eds. (Universitets Forlaget, Oslo, 1970), pp. 175–187.
13. J. J. B. Jack, D. Noble, R. W. Tsien, *Electric Current Flow in Excitable Cells* (Oxford Univ. Press, 1975).
14. C. Koch, T. Poggio, A theoretical analysis of electrical properties of spines. *Proc. R. Soc. London Ser. B* **218**, 455–477 (1983). Medline
15. C. Koch, A. Zador, T. H. Brown, Dendritic spines: Convergence of theory and experiment. *Science* **256**, 973–974 (1992). doi:10.1126/science.1589781 Medline
16. D. Johnston, S. M.-S. Wu, *Foundations of Cellular Neurophysiology* (MIT Press, 1995).
17. D. Tsay, R. Yuste, On the electrical function of dendritic spines. *Trends Neurosci.* **27**, 77–83 (2004). doi:10.1016/j.tins.2003.11.008 Medline
18. R. Yuste, Electrical compartmentalization in dendritic spines. *Annu. Rev. Neurosci.* **36**, 429–449 (2013). doi:10.1146/annurev-neuro-062111-150455 Medline
19. Y. Bando, C. Grimm, V. H. Cornejo, R. Yuste, Genetic voltage indicators. *BMC Biol.* **17**, 71 (2019). doi:10.1186/s12915-019-0682-0 Medline
20. M. Nuriya, J. Jiang, B. Nemet, K. B. Eisenthal, R. Yuste, Imaging membrane potential in dendritic spines. *Proc. Natl. Acad. Sci. U.S.A.* **103**, 786–790 (2006). doi:10.1073/pnas.0510092103 Medline
21. M. A. Popovic, X. Gao, N. T. Carnevale, D. Zecevic, Cortical dendritic spine heads are not electrically isolated by the spine neck from membrane potential signals in parent dendrites. *Cereb. Cortex* **24**, 385–395 (2014). doi:10.1093/cercor/bhs320 Medline
22. T. Kwon, M. Sakamoto, D. S. Peterka, R. Yuste, Attenuation of synaptic potentials in dendritic spines. *Cell Rep.* **20**, 1100–1110 (2017). doi:10.1016/j.celrep.2017.07.012 Medline
23. C. D. Acker, E. Hoyos, L. M. Loew, EPSPs measured in proximal dendritic spines of cortical pyramidal neurons. *eNeuro* **3**, ENEURO.0050-15.2016 (2016). doi:10.1523/ENEURO.0050-15.2016 Medline
24. K. Svoboda, D. W. Tank, W. Denk, Direct measurement of coupling between dendritic spines and shafts. *Science* **272**, 716–719 (1996). doi:10.1126/science.272.5262.716 Medline

25. B. L. Bloodgood, B. L. Sabatini, Neuronal activity regulates diffusion across the neck of dendritic spines. *Science* **310**, 866–869 (2005). doi:10.1126/science.1114816 Medline
26. R. Araya, K. B. Eisenthal, R. Yuste, Dendritic spines linearize the summation of excitatory potentials. *Proc. Natl. Acad. Sci. U.S.A.* **103**, 18799–18804 (2006). doi:10.1073/pnas.0609225103 Medline
27. R. Araya, J. Jiang, K. B. Eisenthal, R. Yuste, The spine neck filters membrane potentials. *Proc. Natl. Acad. Sci. U.S.A.* **103**, 17961–17966 (2006). doi:10.1073/pnas.0608755103 Medline
28. B. L. Bloodgood, A. J. Giessel, B. L. Sabatini, Biphasic synaptic Ca influx arising from compartmentalized electrical signals in dendritic spines. *PLOS Biol.* **7**, e1000190 (2009). doi:10.1371/journal.pbio.1000190 Medline
29. M. T. Harnett, J. K. Makara, N. Spruston, W. L. Kath, J. C. Magee, Synaptic amplification by dendritic spines enhances input cooperativity. *Nature* **491**, 599–602 (2012). doi:10.1038/nature11554 Medline
30. J. Tønnesen, G. Katona, B. Rózsa, U. V. Nägerl, Spine neck plasticity regulates compartmentalization of synapses. *Nat. Neurosci.* **17**, 678–685 (2014). doi:10.1038/nn.3682 Medline
31. R. Araya, T. P. Vogels, R. Yuste, Activity-dependent dendritic spine neck changes are correlated with synaptic strength. *Proc. Natl. Acad. Sci. U.S.A.* **111**, E2895–E2904 (2014). doi:10.1073/pnas.1321869111 Medline
32. K. Jayant, J. J. Hirtz, I. J.-L. Plante, D. M. Tsai, W. D. A. M. De Boer, A. Semonche, D. S. Peterka, J. S. Owen, O. Sahin, K. L. Shepard, R. Yuste, Targeted intracellular voltage recordings from dendritic spines using quantum-dot-coated nanopipettes. *Nat. Nanotechnol.* **12**, 335–342 (2017). doi:10.1038/nnano.2016.268 Medline
33. F. St-Pierre, J. D. Marshall, Y. Yang, Y. Gong, M. J. Schnitzer, M. Z. Lin, High-fidelity optical reporting of neuronal electrical activity with an ultrafast fluorescent voltage sensor. *Nat. Neurosci.* **17**, 884–889 (2014). doi:10.1038/nn.3709 Medline
34. V. Villette, M. Chavarha, I. K. Dimov, J. Bradley, L. Pradhan, B. Mathieu, S. W. Evans, S. Chamberland, D. Shi, R. Yang, B. B. Kim, A. Ayon, A. Jalil, F. St-Pierre, M. J. Schnitzer, G. Bi, K. Toth, J. Ding, S. Dieudonné, M. Z. Lin, Ultrafast two-photon imaging of a high-gain voltage indicator in awake behaving mice. *Cell* **179**, 1590–1608.e23 (2019). doi:10.1016/j.cell.2019.11.004 Medline
35. G. G. Gross, J. A. Junge, R. J. Mora, H.-B. Kwon, C. A. Olson, T. T. Takahashi, E. R. Liman, G. C. R. Ellis-Davies, A. W. McGee, B. L. Sabatini, R. W. Roberts, D. B. Arnold, Recombinant probes for visualizing endogenous synaptic proteins in living neurons. *Neuron* **78**, 971–985 (2013). doi:10.1016/j.neuron.2013.04.017 Medline
36. C. R. Rose, Y. Kovalchuk, J. Eilers, A. Konnerth, Two-photon Na^+ imaging in spines and fine dendrites of central neurons. *Pflugers Arch.* **439**, 201–207 (1999). Medline
37. L. M. Palmer, G. J. Stuart, Membrane potential changes in dendritic spines during action potentials and synaptic input. *J. Neurosci.* **29**, 6897–6903 (2009). doi:10.1523/JNEUROSCI.5847-08.2009 Medline
38. A. M. Packer, D. S. Peterka, J. J. Hirtz, R. Prakash, K. Deisseroth, R. Yuste, Two-photon optogenetics of dendritic spines and neural circuits. *Nat. Methods* **9**, 1202–1205 (2012). doi:10.1038/nmeth.2249 Medline
39. N. C. Klapoetke, Y. Murata, S. S. Kim, S. R. Pulver, A. Birdsey-Benson, Y. K. Cho, T. K. Morimoto, A. S. Chuong, E. J. Carpenter, Z. Tian, J. Wang, Y. Xie, Z. Yan, Y. Zhang, B. Y. Chow, B. Surek, M. Melkonian, V. Jayaraman, M. Constantine-Paton, G. K.-S. Wong, E. S. Boyden, Independent optical excitation of distinct neural populations. *Nat. Methods* **11**, 338–346 (2014). doi:10.1038/nmeth.2836 Medline
40. C. Koch, A. Zador, The function of dendritic spines: Devices subserving biochemical rather than electrical compartmentalization. *J. Neurosci.* **13**, 413–422 (1993). doi:10.1523/JNEUROSCI.13-02-00413.1993 Medline
41. R. Yuste, M. J. Gutnick, D. Saar, K. D. Delaney, D. W. Tank, Ca^{2+} accumulations in dendrites of neocortical pyramidal neurons: An apical band and evidence for two functional compartments. *Neuron* **13**, 23–43 (1994). doi:10.1016/0896-6273(94)90457-X Medline
42. J. Schiller, Y. Schiller, G. Stuart, B. Sakmann, Calcium action potentials restricted to distal apical dendrites of rat neocortical pyramidal neurons. *J. Physiol.* **505**, 605–616 (1997). doi:10.1111/j.1469-7793.1997.605ba.x Medline
43. K. Holthoff, Y. Kovalchuk, R. Yuste, A. Konnerth, Single-shock LTD by local dendritic spikes in pyramidal neurons of mouse visual cortex. *J. Physiol.* **560**, 27–36 (2004). doi:10.1113/jphysiol.2004.072678 Medline
44. H. Jia, N. L. Rochefort, X. Chen, A. Konnerth, Dendritic organization of sensory input to cortical neurons in vivo. *Nature* **464**, 1307–1312 (2010). doi:10.1038/nature08947 Medline
45. T. W. Chen, T. J. Wardill, Y. Sun, S. R. Pulver, S. L. Renninger, A. Baohan, E. R. Schreiter, R. A. Kerr, M. B. Orger, V. Jayaraman, L. L. Looger, K. Svoboda, D. S. Kim, Ultrasensitive fluorescent proteins for imaging neuronal activity. *Nature* **499**, 295–300 (2013). doi:10.1038/nature12354 Medline
46. D. E. Wilson, D. E. Whitney, B. Scholl, D. Fitzpatrick, Orientation selectivity and the functional clustering of synaptic inputs in primary visual cortex. *Nat. Neurosci.* **19**, 1003–1009 (2016). doi:10.1038/nn.4323 Medline
47. I. Segev, W. Rall, Computational study of an excitable dendritic spine. *J. Neurophysiol.* **60**, 499–523 (1988). doi:10.1152/jn.1988.60.2.499 Medline
48. R. Araya, V. Nikolenko, K. B. Eisenthal, R. Yuste, Sodium channels amplify spine potentials. *Proc. Natl. Acad. Sci. U.S.A.* **104**, 12347–12352 (2007). doi:10.1073/pnas.0705282104 Medline
49. N. L. Golding, N. Spruston, Dendritic sodium spikes are variable triggers of axonal action potentials in hippocampal CA1 pyramidal neurons. *Neuron* **21**, 1189–1200 (1998). doi:10.1016/S0896-6273(00)80635-2 Medline
50. D. Holcman, Z. Schuss, Diffusion laws in dendritic spines. *J. Math. Neurosci.* **1**, 10 (2011). doi:10.1186/2190-8567-1-10 Medline
51. T. Lagache, K. Jayant, R. Yuste, Electrodiffusion models of synaptic potentials in dendritic spines. *J. Comput. Neurosci.* **47**, 77–89 (2019). doi:10.1007/s10827-019-00725-5 Medline
52. R. Yuste, Dendritic spines and distributed circuits. *Neuron* **71**, 772–781 (2011). doi:10.1016/j.neuron.2011.07.024 Medline
53. W. Rall, in *Studies in Neurophysiology*, R. Porter, Ed. (Cambridge Univ. Press, 1974), pp. 203–209.
54. M. London, M. Häusser, Dendritic computation. *Annu. Rev. Neurosci.* **28**, 503–532 (2005). doi:10.1146/annurev.neuro.28.061604.135703 Medline
55. D. P. Purpura, Dendritic spine "dysgenesis" and mental retardation. *Science* **186**, 1126–1128 (1974). doi:10.1126/science.186.4169.1126 Medline
56. Y. Bando, M. Sakamoto, S. Kim, I. Ayzenshtat, R. Yuste, Comparative evaluation of genetically encoded voltage indicators. *Cell Rep.* **26**, 802–813.e4 (2019). doi:10.1016/j.celrep.2018.12.088 Medline
57. H. J. Suk, I. van Welie, S. B. Kodandaramaiah, B. Allen, C. R. Forest, E. S. Boyden, Closed-loop real-time imaging enables fully automated cell-targeted patch-clamp neural recording in vivo. *Neuron* **96**, 244–245 (2017). doi:10.1016/j.neuron.2017.09.012 Medline
58. S. Sachidhanandam, V. Sreenivasan, A. Kyriakatos, Y. Kremer, C. C. Petersen, Membrane potential correlates of sensory perception in mouse barrel cortex. *Nat. Neurosci.* **16**, 1671–1677 (2013). doi:10.1038/nn.3532 Medline
59. P. Thévenaz, U. E. Ruttimann, M. Unser, A pyramid approach to subpixel registration based on intensity. *IEEE Trans. Image Process.* **7**, 27–41 (1998). doi:10.1109/83.650848 Medline
60. E. K. Buchanan, I. Kinsella, D. Zhou, R. Zhu, P. Zhou, F. Gerhard, J. Ferrante, Y. Ma, S. Kim, M. Shaik, Y. Liang, R. Lu, J. Reimer, P. Fahey, T. Muhammad, G. Dempsey, E. Hillman, N. Ji, A. Tolias, L. Paninski, Penalized matrix decomposition for denoising, compression, and improved demixing of functional imaging data. bioRxiv 334706 [Preprint] (2019); https://doi.org/10.1101/334706.
61. B. Li, M. Chavarha, Y. Kobayashi, S. Yoshinaga, K. Nakajima, M. Z. Lin, T. Inoue, Two-photon voltage imaging of spontaneous activity from multiple neurons reveals network activity in brain tissue. *iScience* **23**, 101363 (2020). doi:10.1016/j.isci.2020.101363 Medline
62. J. F. Staiger, C. C. H. Petersen, Neuronal circuits in barrel cortex for whisker sensory perception. *Physiol. Rev.* **101**, 353–415 (2021). doi:10.1152/physrev.00019.2019 Medline
63. C. M. Constantinople, R. M. Bruno, Effects and mechanisms of wakefulness on local cortical networks. *Neuron* **69**, 1061–1068 (2011). doi:10.1016/j.neuron.2011.02.040 Medline
64. F. Matyas, V. Sreenivasan, F. Marbach, C. Wacongne, B. Barsy, C. Mateo, R. Aronoff, C. C. H. Petersen, Motor control by sensory cortex. *Science* **330**, 1240–1243 (2010). doi:10.1126/science.1195797 Medline

ACKNOWLEDGMENTS

We thank William Stoy for comments and data in Fig. 1C and S2C. R.Y. is an Ikerbasque Research Professor at the Donostia International Physics Center. Dedicated to the memory of Amiram Grinvald. **Funding:** NINDS grant R01NS110422 (RY), NINDS grant R34NS116740 (RY), NIMH grant R01MH115900 (RY), and PEW Latin American Fellows Program in Biomedical Sciences (VHC). **Author contributions:** Conceptualization: VHC, RY; Methodology: VHC, RY; Software: VHC, NO; Formal Analysis: VHC, NO; Investigation: VHC; Writing – Original Draft: VHC, RY; Writing – Review and Editing: VHC, NO, RY; Visualization: VHC; Supervision: RY; Project administration: RY; Funding acquisition: RY. **Competing interests:** The authors declare no competing interests. **Data and materials availability:** All data are available in the manuscript and the supplementary materials.

SUPPLEMENTARY MATERIALS

science.org/doi/10.1126/science.abg0501

Materials and Methods
Supplementary Text
Figs. S1 to S12
References (*56*–*64*)
MDAR Reproducibility Checklist
Movies S1 and S2

11 December 2020; accepted 1 November 2021
Published online 11 November 2021
10.1126/science.abg0501

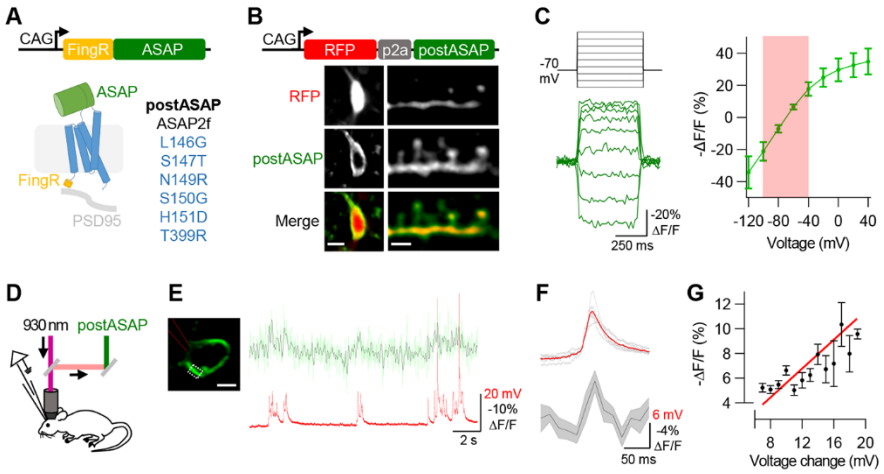

Fig. 1. Characterization of postASAP. (**A**) Construction of postASAP. (**B**) Two-photon imaging of neurons expressing RFP-p2a-postASAP. Left: somatic expression, scale=15 µm. Right: dendritic expression, scale=3 µm. (**C**) Sensitivity of postASAP in ND7/23 cells to 500 ms voltage steps (mean±std; n=5 cells). Red area corresponds to linear range: y=0.6x, R^2=0.9973, p=0.0014. (**D**) Experimental design. (**E**) Left: Patched neuron expressing postASAP (red: pipette outline). White dotted square shows ROI for fluorescence measurement, scale=5 µm. Right: representative optical trace of postASAP (light green: raw fluorescence, black: 10 Hz low-pass filtered) and electrical recording (red). (**F**) Average somatic electrical subthreshold signals (red, 6 events) and simultaneous fluorescence changes (black/gray, mean±std). (**G**) Correlation of peak postASAP fluorescent changes and subthreshold electrical amplitude (mean±std); n=317 subthreshold events, 14 cell, 8 animals; linear regression (red): y=0.58x, confidence interval=[0.55-0.61], R^2=0.7156, p=0.0003.

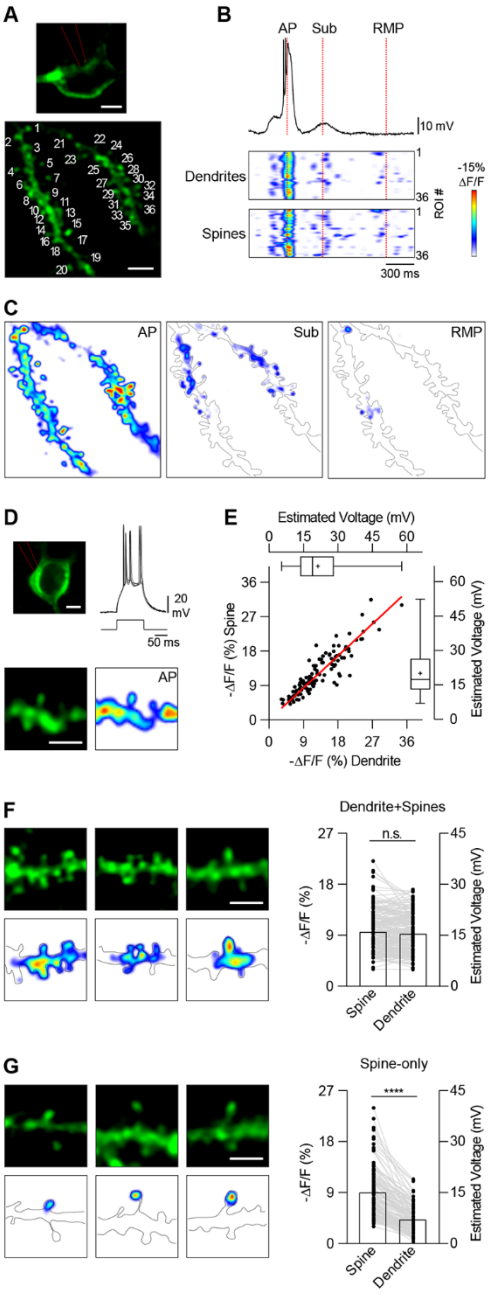

Fig. 2. Spine and dendritic voltage dynamics in vivo during spontaneous activity. (**A**) Top: In vivo two-photon imaging and somatic whole-cell of neurons expressing postASAP (red: pipette outline). Bottom: imaged dendrites (43 µm from center of the image to cell body) of patched cell, scales=5 µm. (**B**) Top: somatic electrical recording of neuron in (A). AP: train of APs; Sub: subthreshold depolarization; RMP: resting membrane potential. Bottom, simultaneous fluorescence changes of numbered spines and adjacent dendrites in (A). (**C**) Representative image with peak fluorescence changes in dendrites and spines during three conditions in (B). (**D**) Depolarization during APs, generated by three 100 ms current pulses (300 pA). Top: somatic imaging and electrophysiological recording. Bottom: representative fluorescence changes in dendrite [average 3 trials; spine at 48 µm from cell body, scale=5 µm; color scale same as (B)]. (**E**) Peak spine and dendrite fluorescence changes during AP trains (n=125 spines, 37 dendrite segments, 5 cells, 4 animals; linear regression: y=0.93x, R^2=0.823, p<0.0001). (**F**) Left: examples Dendrite+Spines patterns (average 10 events). Right: peak fluorescence changes in spine heads and adjacent dendrites (n=221 spines, 90 dendritic segments, 13 cells, 7 animals). (**G**) Same as (F) for Spine-only pattern (n=116 spines, 90 dendritic segments, 13 cells, 7 animals).

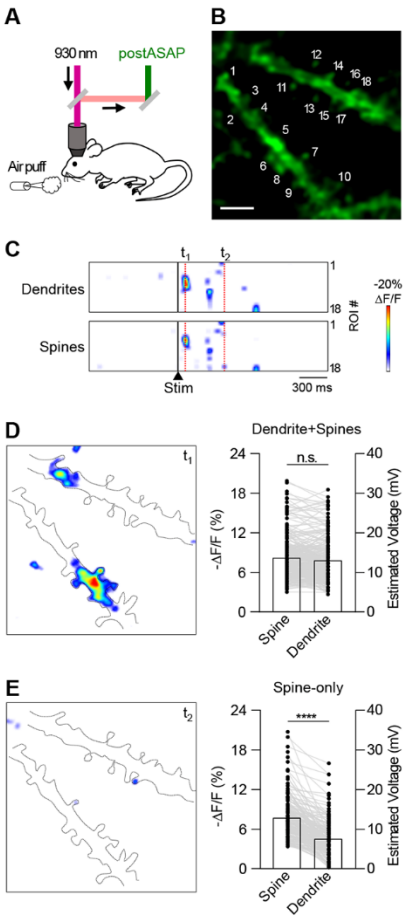

Fig. 3. Spine and dendritic voltage dynamics in vivo after sensory stimulation. (**A**) Experimental design. (**B**) Representative image of dendrites and spines expressing postASAP, scale=5 μm. (**C**) Simultaneous fluorescence changes of numbered spines and adjacent dendrites in (B). (**D**) Left: example image with peak fluorescence changes in dendrites and spines in the time point indicated in (C). Right: peak fluorescence changes in spine heads and adjacent dendrites for Dendrite+Spines pattern (n=255 spines, 49 dendrite segments, 5 animals). (**E**) Same as (D) for Spine-only events (n=181 spines, 49 dendrites, 5 animals).

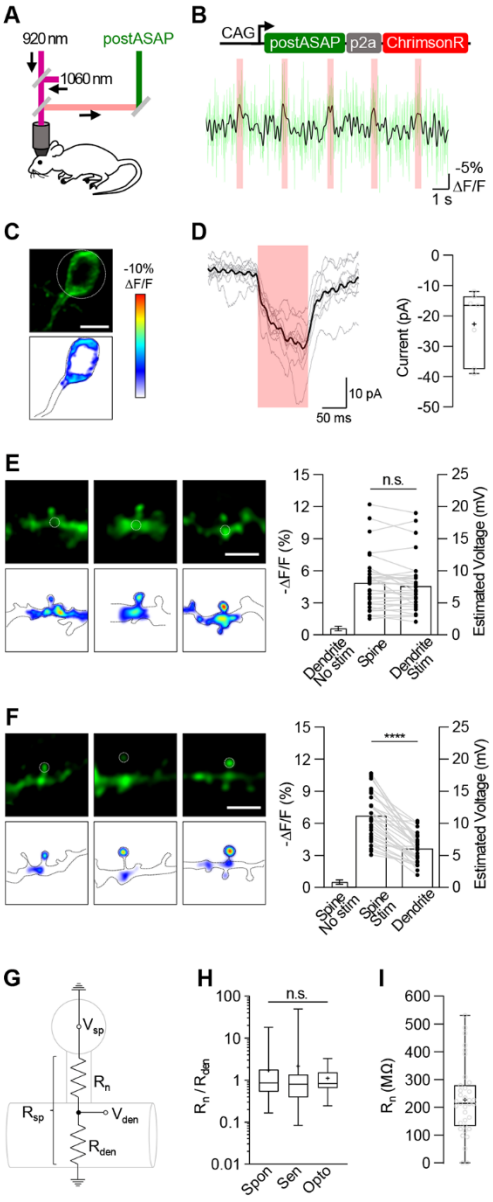

Fig. 4. Two-photon optogenetics and voltage imaging in vivo. (**A**) Experimental design. (**B**) Construct and representative postASAP fluorescence changes in soma (light green: raw fluorescence, black: 10 Hz low-pass filtered) during 500 ms stimulation trials (red, 100 mW power). (**C**) Representative soma and peak fluorescence response during stimulation trials (x10, 500 ms, 100 mW). Dotted circle shown stimulation area, scale=10 µm. (**D**) Left: representative in vivo voltage-clamp recordings during optogenetic stimulation of proximal dendrites (100 mW, 100 ms). Right: Peak currents -22.7 ± 11.3 pA (mean±std), 10 trials (n=7 cells, 4 animals). (**E**) Left: Representative peak fluorescence changes during optogenetic activation of dendritic shafts. Stimulation ROIs in white circle, 10 trials, 100 ms, 100 mW; color bar same as (C), scales=5 µm. Right: peak fluorescence changes in stimulated dendritic shaft (dendrite stim), adjacent dendritic spine (spine); and unstimulated dendritic shaft (dendrite no stim), n=34 dendrites, 9 animals. (**F**) Same as (E) during optogenetic activation of spines, n=35 spines, 12 animals. (**G**) Simplified electrical model. V_{sp}: spine voltage; R_n: neck resistance; V_{den}: dendritic voltage; R_{den}: dendritic resistance; R_{sp}: spine input resistance. (**H**) Resistances ratio (R_n to R_{den}) of Spine-only events during spontaneous (n=116), sensory stimuli (n=181) and optogenetic spine stimulation (n=35). (**I**) Values of spine neck resistance (R_n) for stimulated spines; median=213.7 MΩ (n=35 spines).

Voltage compartmentalization in dendritic spines in vivo

Victor Hugo CornejoNetanel OferRafael Yuste

Science, **Ahead of Print** • DOI: 10.1126/science.abg0501